Title

Resistance-gene-directed discovery of a natural-product herbicide with a new mode of action.

Journal

Nature, 559(7714)

ISSN

0028-0836

Authors

Yan, Yan
Liu, Qikun
Zang, Xin
et al.

Publication Date

2018-07-01

DOI

10.1038/s41586-018-0319-4

Peer reviewed

Published in final edited form as:

Nature. 2018 July ; 559(7714): 415–418. doi:10.1038/s41586-018-0319-4.

Resistance-Gene Directed Discovery of a Natural Product Herbicide with a New Mode of Action

Yan Yan[1,†], **Qikun Liu**[2,†], **Xin Zang**[†,4,7], **Shuguang Yuan**[5], **Undramaa Bat-Erdene**[1], **Calvin Nguyen**[2], **Jianhua Gan**[6], **Jiahai Zhou**[4,7,*], **Steven E. Jacobsen**[2,*], and **Yi Tang**[1,3,*]

[1]Department of Chemical and Biomolecular Engineering, University of California Los Angeles, CA 90095 (USA) [2]Department of Molecular, Cell, and Developmental Biology, and Howard Hughes Medical Institute, University of California Los Angeles, CA 90095 (USA) [3]Department of Chemistry and Biochemistry, University of California Los Angeles, CA 90095 (USA) [4]State Key Laboratory of Bio-organic and Natural Products Chemistry, Shanghai Institute of Organic Chemistry, Chinese Academy of Sciences, Shanghai, China [5]Laboratory of Physical Chemistry of Polymers and Membranes, Ecole Polytechnique Fédérale de Lausanne, Lausanne, Switzerland [6]State Key Laboratory of Genetic Engineering, Collaborative Innovation Center of Genetics and Development, Department of Physiology and Biophysics, School of Life Sciences, Fudan University, Shanghai 200433, China [7]Department of Chemistry, Shanghai Normal University, Shanghai 200234, China

Text

Bioactive natural products have evolved to inhibit specific cellular targets and have served as lead molecules for health and agricultural applications for the last century[1–3]. The post-genomics era has brought a renaissance in natural product discovery using synthetic biology tools[4–6]. However, compared to traditional bioactivity-guided approaches, genome mining of natural products with specific and potent biological activities remains challenging[4]. Here we present the discovery and validation of a highly potent herbicide lead that targets a critical metabolic enzyme that is required for plant survival. Our approach is based on the coclustering of a self-resistance gene in the natural product biosynthetic gene cluster[7–9], which serves as a window to potential biological activity of the encoded compound. We

*Correspondence to: yitang@ucla.edu, jacobsen@ucla.edu, jiahai@mail.sioc.ac.cn.

†These authors contributed equally to this work

Correspondence and requests for materials should be addressed to Y.T. (yitang@ucla.edu), S.E.J. (jacobsen@ucla.edu) and J.Z. (jiahai@mail.sioc.ac.cn).

Supplementary Information is available in the online version of the paper.

Author Contributions Y.Y., Q.L., J.Z., S.E.J. and Y.T. developed the hypothesis and designed the study. Y.Y. performed all in vivo and in vitro experiments. Q.L., Y.Y. and C.N. performed plant experiments. X.Z. and J.Z. performed crystallography experiments. J.G. determined the protein structure. S.Y. performed computational experiments. Y.Y. and U.B. performed yeast experiments. Y.Y., Q.L., J.Z., S.E.J. and Y.T. prepared the manuscript.

A PCT patent application related to this manuscript has been filed by UCLA.

Readers are welcome to comment on the online version of the paper.

targeted dihydroxyacid dehydratase (DHAD) in the branched-chain amino acid (BCAA) biosynthetic pathway in plants, the last step in this pathway often targeted for herbicide development[10]. We showed the fungal sesquiterpenoid aspterric acid (AA) discovered using this method is a submicromolar inhibitor of DHAD and is effective as an herbicide in spray applications. The self-resistance gene *astD* was validated to be insensitive to AA and was deployed as a transgene in establishment of plants that are resistant to AA. This herbicide-resistance gene combination complements urgent efforts in overcoming weed resistance[11]. Our discovery demonstrates the potential of using a resistance-gene directed approach in mining of bioactive natural products.

Weeds are a major source of crop losses, and the evolution of herbicide resistance in weeds has led to an urgent need for new herbicides with novel modes of action[11–14]. The BCAAs biosynthetic pathway is essential for plant growth[10]. It is not present in animals and is therefore a validated target for highly specific weed control agents[10]. The BCAA biosynthetic pathway in plants is carried out by three enzymes: acetolactate synthase (ALS), acetohydroxy acid isomeroreductase (KARI), and DHAD (Fig. 1a). Given the success of targeting ALS for herbicide development[11], it is surprising that no herbicide that targets either of the other two enzymes has been developed. DHAD which catalyzes β-dehydration reactions to yield α-keto acid precursors to isoleucine, valine and leucine, is an essential and highly conserved enzyme among plant species[15,16] (Extended Data Fig. 1a and Supplementary Fig. 1). Efforts toward synthetic DHAD inhibitors resulted in compounds with submicromolar K_i; however, the compounds have no *in planta* activity[17] (Extended Data Fig. 1b).

Filamentous fungi are prolific producers of natural products (NPs), many of which have biological activities that aid the fungi in colonizing and killing plants[1,2,18]. Therefore, fungal NPs represent a promising source of potential leads for herbicides. The abundance of sequenced fungal genomes enables genome mining of new NPs with novel biological activities[4,6]. Although no NP inhibitors of DHAD are known to date, we reason a fungal NP with this property might exist, given the indispensable role of BCAA biosynthesis in plants[10].

To identify NP biosynthetic gene clusters that may encode a DHAD inhibitor, we hypothesized that such cluster must contain an additional copy of DHAD that is insensitive to the inhibitor, thereby providing the required self-resistance for the producing organism to survive. The presence of a gene encoding a self-resistance enzyme is frequently found in microbial NP gene clusters, as highlighted by the presence of an insensitive copy of HMGR or IMPDH in the gene clusters for lovastatin (that targets HMGR) or mycophenolic acid (that targets IMPDH), respectively (Extended Data Fig. 1c)[19,20]. This phenomenon has been used to predict molecular targets of NPs, as well as to identify gene clusters of NPs of known activities[5,7,9].

To identify possible self-resistance enzymes, we scanned sequenced fungal genomes to search for colocalizations of genes encoding DHAD with core biosynthetic enzymes, such as terpene cyclases, polyketide synthases, etc[21,22]. We identified a well-conserved set of four genes across multiple fungal genomes (Fig. 1b), including the common soil fungus

Aspergillus terreus that is best known to produce lovastatin. The conserved gene clusters include genes that encode a sesquiterpene cyclase homolog (*astA*), two cytochrome P450s (*astB* and *astC*), and a homolog of DHAD (*astD*). Genes outside of this cluster are not conserved across the identified genomes and are hence unlikely to be involved in NP biosynthesis. AstD is the second copy of DHAD encoded in the genome, and is ~70% similar to the housekeeping copy that is well-conserved across fungi (Supplementary Fig. 2). Therefore, AstD is potentially a self-resistance enzyme that confers resistance to the encoded NP. Like a majority of biosynthetic gene clusters in sequenced fungal genomes, the *ast* cluster has not been associated with the production of a known NP[4].

To identify the NP encoded by the *ast* cluster, we heterologously expressed *astA, astB,* and *astC* genes in the host *Saccharomyces cerevisiae* RC01[23]. New compounds that emerged were purified and their structures were elucidated with NMR spectroscopy (Supplementary Fig. 3 and Supplementary Table 5). RC01 expressing only *astA* produced a new sesquiterpene (**1**), which was confirmed to be (−)-daucane (Supplementary Fig. 4). RC01 expressing both *astA* and *astB* led to the biosynthesis of a new product that was structurally determined to be the α-epoxy carboxylate (**2**) (Fig. 1c). When *astA*, *astB* and *astC* were expressed together, a new compound (**3**) became the dominant product (~ 20 mg/L). Full structural determination revealed the compound to be the tricyclic aspterric acid (**AA**), which is a previously isolated compound (Fig. 1c)[24]. The biosynthetic pathway for **AA** is therefore concise: following cyclization of farnesyl diphosphate by AstA to create the carbon skeleton in **1**, AstB catalyzes oxidation of **1** to yield the epoxide **2.** Further oxidation by AstC at carbon 15 yields an alcohol, which can undergo intramolecular epoxide opening to create **AA** (Fig. 1d).

Upon its initial discovery, **AA** was shown to have inhibitory activity towards *Arabidopsis thaliana,* however, the mode of action was not known[25]. Our resistance-gene directed approach led to rediscovery of this compound with DHAD as a potential target. We first confirmed that **AA** is able to potently inhibit *A. thaliana* growth in an agar-based assay (Fig. 2a, and Supplementary Fig. 5). **AA** was also an effective inhibitor of root development and plant growth when applied to a representative monocot (*Zea mays*) and dicot (*Solanum lycopersicum*) (Fig. 2b). To test if **AA** indeed targets DHAD, we expressed and purified housekeeping DHAD from both *A. terreus* (XP_001208445.1, fDHAD) and *A. thaliana* (AT3G23940, pDHAD), as well as the putative self-resistance enzyme AstD (Supplementary Fig. 6). Both housekeeping DHAD enzymes converted dihydroxyisovalerate to ketoisovalerate (pDHAD: k_{cat} = 1.2 sec^{-1}, K_M = 5.7 mM) as expected. The enzyme activities, however, were inhibited in the presence of **AA** (Extended Data Fig. 2). The IC_{50} values of **AA** towards fDHAD and pDHAD were 0.31 μM and 0.50 μM at an enzyme concentration of 0.50 μM, respectively (Extended Data Fig. 3). **AA** was further determined to be a competitive inhibitor of pDHAD with a K_i = 0.30 μM (Extended Data Fig. 3). **AA** displayed no significant cytotoxicity towards human cell lines up to 500 μM concentration, consistent with the lack of DHAD in mammalian cells (Supplementary Fig. 7).

AstD catalyzes the identical β-dehydration reaction as DHAD, albeit with a significantly more sluggish turnover rate (k_{cat} = 0.03 sec^{-1}, K_M = 5.4 mM). However, the enzyme was not inhibited by **AA**, even at the solubility limit of 8 mM (Extended Data Fig. 3). To determine

if AstD can confer resistance to **AA**-sensitive strains, we developed a yeast based assay. The genome copy of DHAD encoded by *ILV3* was first deleted from *Saccharomyces cerevisiae* strain DHY *ΔURA3*, which resulted in an auxotroph that requires exogenous addition of Ile, Leu and Val to grow. We then introduced either *fDHAD* or *astD* episomally, both of which allowed the strain to grow in the absence of the three BCAAs (Extended Data Fig. 4). However, yeast expressing fDHAD was approximately 100 times more sensitive to **AA** (IC_{50} of 2 μM) compared to yeast expressing AstD (IC_{50} of 200 μM) (Fig. 2c). Collectively, the biochemical and genetic assays validated **AA** as the first natural product inhibitor of fungal and plant DHAD; and AstD serves as the self-resistance enzyme in the *ast* biosynthetic gene cluster.

The (*R*)-α-hydroxyacid and (*R*)-configured β-ether oxygen moieties in **AA** mimic the (*2R, 3R*)-dihydroxy groups present in natural substrates such as dihydroxyisovalerate. The β-ether oxygen in **AA** is in position to coordinate to the 2Fe-2S cluster that is a required cofactor in both fungal and plant DHAD[16,17]. To understand potential **AA** mechanism of action, we determined the crystal structure (2.11 Å) of the pDHAD complexed with 2Fe-2S cluster (*holo*-pDHAD) (Fig. 2d, Extended Data Fig. 5, and Extended Data Table 1). We identified a binding chamber at the homodimer interface, similar to that found in the *holo* bacterial L-arabinonate dehydratase[26] (Fig. 2d). The interior of the chamber is positively charged (2Fe-2S and Mg^{2+}) while the entrance is lined with hydrophobic residues. The modeled binding mode of α,β-dihydroxyisovalerate and **AA** predicted by computational docking are shown in Fig. 2e. The pocket is sufficiently spacious to accommodate the bulkier **AA**, and provide stronger hydrophobic interactions than the native substrate with a 5.3 ± 0.3 kcal/mol gain in binding energy (Fig. 2e). Base on the *holo*-pDHAD structure, we constructed a homology model of AstD to determine potential mechanism of resistance (Extended Data Fig. 5 and 6). Comparison of pDHAD and the modeled AstD structures shows that while most of the residues in the catalytic chamber are conserved, the hydrophobic region at the entrance to the reactive chamber in AstD is more constricted as a result of two amino acid substitutions (V496L and I177L). Narrowing of the entrance could therefore sterically exclude the bulkier **AA** from binding in the active site, while the smaller, natural substrates are still able to enter the chamber.

To explore the potential of **AA** as an herbicide, we performed spray treatment of *A. thaliana* with **AA**. We added **AA** into a commercial glufosinate formulation known as Finale® at a final **AA** concentration of 250 μM[27,28]. We then sprayed **AA** solution onto glufosinate resistant *A. thaliana*. Finale® alone had no observable inhibitory effects on plant growth, but adding **AA** severely inhibited plant growth (Extended Data Fig. 7). In addition, *A. thaliana* plants treated with **AA** before flowering failed to form normal pollen, which was also observed previously[25]. We found that the pistil of treated plants could still be successfully pollinated using healthy pollen from the untreated *A. thaliana,* indicating that **AA** preferentially affects pollen but not egg formation (Extended Data Fig. 8 and 9). This effect was also observed with a lower concentration of **AA** (100 μM). Thus, in addition to its herbicidal properties, **AA** could potentially be used as a chemical hybridization agent for hybrid seed production[29].

We next investigated whether plants expressing *astD* are resistant to **AA**. This was motivated by the successful combination of glyphosate and genetically modified crops that are selectively resistant to glyphosate (Roundup Ready®)[30]. The *A. terreus astD* gene was codon optimized and the *N*-terminus was fused to a chloroplast localization signal derived from pDHAD. Wild type or *astD* transgene-expressing *A. thaliana* was then grown on media that contained 100 μM **AA**. In the presence of **AA**, the growth of wild-type plants was strongly inhibited, and arrested at the cotyledon stage (Fig. 3a). In contrast, the growth of *astD* transgenic plants was relatively unaffected by **AA**, as indicated by the normally expanded rosette leaves, elongated roots, and whole plant fresh weight (Fig. 3a and b). The expression of AstD was verified by western blot (Supplementary Fig. 8). A spray assay was also performed using T2 *astD* transgenic *A. thaliana* plants, which showed no observable growth defects under such treatment (Fig. 3c). In contrast, the control plants carrying the empty vector showed a strong growth inhibitory phenotype when treated with **AA** (Fig. 3c). Quantitative measurements of plant height showed AstD effectively confers **AA** resistance to *A. thaliana* (Fig. 3d).

In summary, resistance-gene directed discovery of NPs in the fungus *A. terreus* led to the discovery of a natural herbicide **AA** and the determination of its mode of action. In addition, introducing *astD* as a transgene or editing the sequence of the plant DHAD endogenous gene could be used to create **AA**-resistant crops. We suggest that **AA** is a promising lead for the development as a broad spectrum commercial herbicide.

METHODS

General materials and methods

Biological reagents, chemicals, media and enzymes were purchased from standard commercial sources unless stated. Plant, fungal, yeast and bacterial strains, plasmids and primers used in this study are summarized in Supplementary Tables 3, 4 and 5. DNA and RNA manipulations were carried out using Zymo ZR Fungal/Bacterial DNA Microprep™ kit and Invitrogen Ribopure™ kit respectively. DNA sequencing was performed at Laragen, Inc. The primers and codon optimized gblocks were synthesized by IDT, Inc.

Expression of *ast* genes in *Aspergillus nidulans* for cDNA isolation

Plasmids pYTU, pYTP, pYTR digested with *Pac*I and *Swa*I were used as vectors to insert genes[31]. A *gpda* promoter was generated by PCR amplification using primers Gpda-pYTU-F and Gpda-R with pYTR serving as template. Genes to be expressed were amplified through PCR using the genomic DNA of *Aspergillus terreus* NIH2624 as a template. A 4.5 kb fragment obtained using primers AstD-pYTU-recomb-F and AstA-pYTU-recomb-R was cloned into pYTU together with a *gpda* promoter by yeast homologous recombination to obtain pAstD+AstA-pYTU. Yeast transformation was performed using Frozen-EZ Yeast Transformation II Kit™ (Zymo Research). A 2.4 kb fragment obtained using primers AstB-pYTR-recomb-F and AstB-pYTR-recomb-R was cloned into pYTR by yeast homologous recombination to obtain pAstB-pYTR. Similarly, a 2.3 kb fragment obtained using primers AstC-pYTP-recomb-F and AstC-pYTP-recomb-R was cloned into pYTP by yeast homologous recombination to obtain pAstC-pYTP.

All three plasmids (pAstD+AstA-pYTU, pAstB-pYTR and pAstC-pYTP) were transformed into *A. nidulans* following standard protocols to result in the *A. nidulans* strain TY01[31]. TY01 was cultured in liquid CD-ST medium (20 g/L starch, 20 g/L peptone, 50 mL/L nitrate salts and 1 mL/L trace elements) at 28°C for 3 days. Total RNA of TY01 was extracted with the Invitrogen Ribopure™ kit, and total cDNA of TY01 was obtained using the SuperScript III reverse transcriptase kit (Thermo Fisher Scientific). The cDNA fragment of *astA* was PCR amplified using primers AstA-xw55-recomb-F and AstA-xw55-recomb-R. The cDNA fragment of *astB* was PCR amplified using primers AstB-xw06-recomb-F and AstB-xw06-recomb-R. The cDNA fragment of *astC* was PCR amplified using primers AstC-xw02-recomb-F and AstC-xw02-recomb-R. The cDNA fragment of *astD* was PCR amplified using primers AstD-pXP318-F and AstD-pXP318-R. All the introns were confirmed to be correctly removed by sequencing.

Construction of *Saccharomyces cerevisiae* strains

Plasmid pXW55 (*URA3* marker) digested with *Nde*I and *Pme*I was used to introduce the *astA* gene[23]. A 1.3 kb fragment containing *astA* obtained from PCR using primers AstA-xw55-recomb-F and AstA-xw55-recomb-R was cloned into pXW55 using yeast homologous recombination to afford pAstA-xw55. The plasmid pAstA-xw55 was then transformed into *Saccharomyces cerevisiae* RC01 to generate strain TY02[23].

Plasmid pXW06 (*TRP1* marker) digested with *Nde*I and *Pme*I was used to introduce the *astB* gene[23]. A 1.6 kb fragment containing *astB* obtained from PCR using primers AstB-xw06-recomb-F and AstB-xw06-recomb-R were cloned into pXW06 using yeast homologous recombination to afford pAstB-xw06. The plasmid pAstB-xw06 was then transformed into TY02 to generate strain TY03.

Plasmid pXW06 (*LEU2* marker) digested with *Nde*I and *Pme*I was used to introduce the *astC* gene[23]. A 1.6 kb fragment containing *astC* obtained from PCR using primers AstC-xw02-recomb-F and AstC-xw02-recomb-R were cloned into pXW02 using yeast homologous recombination to afford pAstC-xw02. The plasmid pAstC-xw02 was then transformed into TY03 to generate strain TY04.

URA3 gene was inserted into *ilv3* locus of *Saccharomyces cerevisiae* DHY Δ*URA3* strain to generate UB01. A 879 bp homologous recombination donor fragment with 35–40 bp homologous regions flanking *ilv3* ORF was amplified using primers ILV3p-URA3-F and ILV3t-URA3-R using yeast gDNA as template. The PCR product was gel purified and transformed into *Saccharomyces cerevisiae* DHY Δ*URA3,* and selected on uracil dropout media to give UB01. The resulting strain was subjected to verification by colony PCR with primers ILV3KO-ck-F and ILV3KO-ck-R and the amplified fragment was sequence confirmed.

The *URA3* gene inserted into *ilv3* locus of *Saccharomyces cerevisiae* DHY Δ*URA3* was deleted from UB01 using homologous recombination to generate UB02. A 150 bp homologous recombination donor fragment with 75 bp homologous regions flanking *ilv3* ORF was amplified using primers ILV3KO-F and ILV3KO-R, gel purified and transformed into UB01, and counterselected on 5-fluoroorotic acid (5-FoA) containing media to give

UB02. The resulting strain was subjected to verification by colony PCR with primers ILV3KO-ck-F and ILV3KO-ck-R and the amplified fragment was sequenced confirmed.

The empty plasmid pXP318 (*URA3* marker) was transformed into UB02 to generate TY05[32].

Plasmid pXP318 digested with *Spe*I and *Xho*I was used as vector to introduce gene encoding fDHAD[32]. The cDNA of *Aspergillus terreus* NIH 2624 served as template for PCR amplification. A 1.7 kb fragment obtained using primers fDHAD-pXP318-F and fDHAD-pXP318-R were cloned into pXP318 using yeast homologous recombination to afford fDHAD-pXP318. Then, fDHAD-pXP318 was transformed into UB02 to generate TY06. fDHAD was driven by a constitutive promoter *TEF1*.

Plasmid pXP318 digested with *Spe*I and *Xho*I was used as vector to introduce *astD* gene[32]. The cDNA isolated from TY01 served as the template for PCR amplification. A 1.8 kb fragment obtained using primers AstD-pXP318-F and AstD-pXP318-R were cloned into pXP318 using yeast homologous recombination to give AstD-pXP318. A FLAG-tag was also add to the *N*-terminal of AstD. Then, AstD-pXP318 was transformed into UB02 to generate TY07. AstD was driven by a constitutive promoter *TEF1*.

Fermentation and compound analyses and isolation

A seed culture of *S. cerevisiae* strain was grown in 40 mL of synthetic dropout medium for 2 d at 28°C, 250 rpm. Fermentation of the yeast was carried out using YPD (yeast extract 10 g/L, peptone 20 g/L) supplement with 2% dextrose for 3 d at 28°C, 250 rpm.

HPLC-MS analyses were performed using a Shimadzu 2020 EVLC-MS (Phenomenex® Luna, 5μ, 2.0 × 100 mm, C-18 column) using positive and negative mode electrospray ionization. The elution method was a linear gradient of 5–95% (v/v) acetonitrile/water in 15 min, followed by 95% (v/v) acetonitrile/water for 3 min with a flow rate of 0.3 mL/min. The HPLC buffers were supplemented with 0.05% formic acid (v/v). HPLC purifications were performed using a Shimadzu Prominence HPLC (Phenomenex® Kinetex, 5μ, 10.0 × 250 mm, C-18 column). The elution method was a linear gradient of 65–100% (v/v) acetonitrile/water in 25 min, with a flow rate of 2.5 mL/min. GC-MS analyses were performed using Agilent Technologies GC-MS 6890/5973 equipped with a DB-FFAP column. An inlet temperature of 240°C and constant pressure of 4.2 psi were used. The oven temperature was initially at 60°C and then ramped at 10°C/min for 20 min, followed by a hold at 240°C for 5 min.

To isolate compound **1**, the fermentation broth of TY02 was centrifuged (5000 rpm, 10 min), and cell pellet was harvested and soaked in acetone. The organic phase was dried over sodium sulfate, concentrated to oil form, and subjected to silica column purification with hexane. To isolate compound **2**, the fermentation broth of TY03 was centrifuged (5000 rpm, 10 min), and supernatant was extracted three times with ethyl acetate. The organic phase was dried over sodium sulfate, concentrated to oil form, and then and subjected to HPLC purification. To isolate compound **AA**, the fermentation broth of TY04 was centrifuged (5000 rpm, 10 min), and supernatant was extracted three times with ethyl acetate. The

organic phase was dried over sodium sulfate, concentrated to oil form, and subjected to HPLC purification.

Structure determination of compounds

Compound **1**, colorless oil readily dissolved in hexane and chloroform, had a molecular formula $C_{15}H_{24}$, as deduced from EI-MS $[M]^+$ *m/z* 204, and showed $[\alpha]_D^{22} = -30°$ (*n*-hexane; *c* = 0.1). GC-MS 70 eV, *m/z* (relative intensity): 204 $[M]^+$ (42), 189 (5), 161 (35), 136 (100), 133 (10), 121 (70), 119 (25), 107 (20), 105 (27), 93 (21), 91 (26), 79 (13), 77 (15), 69 (20), 55 (12), 43 (12), 41 (13), 38 (21); ^{1}H NMR (500 MHz, $CDCl_3$): δ 5.37 (1H, m), 2.20-2.10 (5H, m), 2.10-2.00 (2H, m), 1.95 (1H, d, 15.3), 1.75 (3H, s), 1.71 (3H, q, 1.7), 1.61 (3H, brs), 1.44 (1H, dd, 11.4, 7.2), 1.36 (1H, m), 1.31 (1H, dd, 11.3, 2.6), 0.73 (3H, s); ^{13}C NMR (125 MHz, $CDCl_3$): δ 138.4, 138.3, 122.4, 122.2, 57.4, 42.6, 41.4, 40.3, 34.5, 29.6, 27.3, 25.0, 23.3, 20.6, 19.2. Both of the NMR and MS spectrums are identical to a known compound (+)-daucane, however, the optical rotation is opposite which led to the assignment of **1** to be (−)-daucane[33].

Compound **2**, colorless oil readily dissolved in ethyl acetate and chloroform, had a molecular formula $C_{15}H_{22}O_3$, as deduced from LC-MS $[M+H]^+$ *m/z* 251, $[M-H]^-$ *m/z* 249. ^{1}H NMR (500 MHz, $CDCl_3$): δ 8.09 (1H, brs), 3.25 (1H, t, 7.4), 2.71 (1H, dd, 14.6, 6.5), 2.48 (1H, dd, 14.8, 6.3), 2.36 (1H, dd, 14.0, 6.6), 2.26 (1H, m), 2.15 (1H, dd, 16.3, 8.9), 2.08 (1H, d, 12.0), 1.84 (1H, q, 13.1), 1.73 (3H, d, 2.3), 1.59 (3H, d, 2.2), 1.48~1.35 (3H, m), 1.31 (1H, td, 11.5, 9.0), 0.86 (3H, s). ^{13}C NMR (125 MHz, $CDCl_3$): δ 176.0, 135.8, 123.2, 60.1, 59.8, 59.4, 44.1, 40.5, 38.8, 30.6, 29.3, 24.9, 23.8, 20.6, 17.8.

Compound **3** is a colorless oil readily dissolved in acetone and chloroform, had a molecular formula $C_{15}H_{22}O_4$, as deduced from LC-MS $[M+H]^+$ *m/z* 267, $[M-H]^-$ *m/z* 265. ^{1}H NMR (500 MHz, $CDCl_3$): δ 4.29 (1H, d, 8.5), 3.92 (1H, d, 8.3), 3.48 (1H, d, 8.3), 2.42 (1H, dd, 14.9, 7.3), 2.37~2.28 (2H, m), 2.25 (1H, dd, 13.0, 4.4), 2.20~2.17 (1H, m), 2.12 (1H, d, 13.4), 2.01 (1H, m), 1.80~1.65 (2H, m), 1.71 (3H, s), 1.64~1.54 (1H,m), 1.60 (3H, s), 1.50 (1H, m); ^{13}C NMR (125 MHz, $CDCl_3$): δ 178.2, 134.5, 125.2, 82.9, 76.3, 75.6, 55.4, 53.0, 36.6, 36.2, 33.8, 32.2, 23.6, 23.4, 20.9. **3** is identical to aspterric acid (**AA**) as reported[24,25].

Protein expression, purification and biochemical assay

To express and purify pDHAD, primers pDHAD-pET-F and pDHAD-pET-R were used to amplify a 1.7 kb DNA fragment containing *pdhad* (AT3G23940). The PCR product was cloned into pET28a using *Nhe*I and *Not*I restriction sites. The resulting plasmid pDHAD-pET was transformed into *E.coli* BL21 (DE3) to give TY08. To express and purify fDHAD (XP_001208445.1), primers fDHAD-pET-F and fDHAD-pET-R were used to amplify a 1.6 kb DNA fragment containing *fdhad*. The PCR product was cloned into pET28a using *Nde*I and *Not*I restriction sites. The resulted plasmid fDHAD-pET was transformed into *E. coli* BL21 (DE3) to obtain TY09. To express and purify AstD (XP_001213593.1), primers AstD-pET-F and AstD-pET-R were used to amplify a 1.6 kb DNA fragment containing *astD*. The PCR product was cloned into pET28a using *Nde*I and *Not*I restriction sites. The resulted plasmid AstD-pET was transformed into *E. coli* BL21 (DE3) to obtain TY10. All DHADs fused a 6×His-tag with a molecular weight ~62 kD were expressed at 16°C 220 rpm for 20 h

after 100 μM IPTG induction (IPTG was added when OD_{600} = 0.8). Cells of 1 L culture were then harvested by centrifugation at 5000 rpm at 4°C. Cell pellet was resuspended in 15 mL Buffer A10 (20 mM Tris-HCl pH 7.5, 50 mM NaCl, 8% glycerol, 10 mM imidazole). The cells were lysed by sonication, and the insoluble material was sedimented by centrifugation at 16000 rpm at 4°C. The protein supernatant was then incubated with 3 mL Ni-NTA for 4 h with slow, constant rotation at 4°C. Subsequently the Ni-NTA resin was washed with 10 column volumes of Buffer A50 (Buffer A + 50 mM imidazole). For elution of the target protein, the Ni-NTA resin was incubated for 10 min with 6 mL Buffer A300 (Buffer A + 300 mM imidazole). The supernatant from the elution step was then analyzed by SDS-PAGE together with the supernatants from the other purification steps. The elution fraction containing the recombinant protein was buffer exchanged into storage buffer (50 mM Tris-HCl pH 7.2, 50 mM NaCl, 10 mM $MgCl_2$, 10% glycerol, 5 mM DTT, 5 mM GSH).

In vitro activity assays were carried out in 50 μL reaction mixture containing storage buffer, 10 mM (±)-sodium α,β-dihydroxyisovalerate hydrate (**4**) and 0.5 μM of purified DHAD enzyme. The reaction was initiated by adding the enzyme. After 0.5 h incubation at 30°C, the reactions were stopped by adding equal volume of ethanol. Approximately 0.1 volume of 100 mM phenylhydrazine (PHH) was added to derivatize the product 3-methyl-2-oxo-butanoic acid (**5**) into **6** at room temperature for 30 min. 20 μL of the reaction mixture was subject to LC-MS analysis. The area of the HPLC peak with UV absorption at 350 nm were used to quantify the amount of **6**. (Extended Data Fig. 2).

The inhibition percentage of **AA** on DHADs determined using *in vitro* biochemical assays are calculated by following equation:

$$\text{inhibition percentage} = 1 - \frac{\text{initial reaction rate with } \mathbf{AA}}{\text{initial reaction rate without } \mathbf{AA}}$$

Growth inhibition assay of *S. cerevisiae* on plates or in the tubes

S. cerevisiae was grown in isoleucine, leucine and valine (ILV) dropout media (20 g/L glucose, 0.67 g/L Difco™ Yeast Nitrogen Base w/o amino acids, 18 mg/L adenine, arginine 76 mg/L, asparagine 76 mg/L, aspartic acid 76 mg/L, glutamic acid 76 mg/L, histidine 76 mg/L, lysine 76 mg/L, methionine 76 mg/L, phenylalanine 76 mg/L, serine 76 mg/L, threonine 76 mg/L, tryptophan 76 mg/L, tyrosine 76 mg/L) to test growth inhibition of **AA** on *S. cerevisiae. S. cerevisiae* was incubated at 28°C until OD_{600} of the control strain without **AA** treatment reached about 0.8. The ratio of yeast OD_{600} in media with **AA** treatment to yeast OD_{600} in media without **AA** was calculated as the percentage of growth inhibition. The inhibition curve was plotted as percentage of inhibition versus **AA** concentrations. To further prove **AA** affects BCAA biosynthesis, isoleucine, leucine and valine was also complemented to the media with or without treatment of **AA**. The growth curves of TY05, TY06 and TY07 were also plotted in Extended Data Fig. 4. The OD_{600} was recorded for every 20 min over a total of 50 h. Percent inhibition. The growth inhibition percentage of **AA** on *S. cerevisiae* strain is calculated by dividing the cell density (OD_{600}) of

the **AA**-treated strain to the corresponding untreated strains when OD_{600} reaches ~ 0.8 using following equation:

$$\text{growth inhibition percentage} = 1 - \frac{OD_{600} \text{ of } \mathbf{AA} \text{ treated strain}}{0.8}$$

in which 0.8 is the OD_{600} of untreated strain.

Growth inhibition assay of plants on plates or in the tubes

MS (2.16 g/L Murashige and Skoog basal medium, 8 g/L sucrose, 8 g/L agar) media was used to test the growth inhibition of **AA** on *A. thaliana*, *Solanum lycopersicum,* and *Zea mays. A. thaliana*, *S. lycopersicum,* and *Z. mays* were grown under long day condition (16/8 h light/dark) using cool-white fluorescence bulbs as the light resource at 23°C. **AA** was dissolved in ethanol and added to the media before inoculating strains or growing plants. The media of control treatment contains the same amount of ethanol, but without **AA**.

Plant growth inhibition assay by spraying

AA was firstly dissolved in ethanol and then added to solvent (0.06 g/L Finale® Bayer Inc. + 20 g/L EtOH). The control plants were treated with solvent containing ethanol only. *A. thaliana* that are resistant to glufosinate (containing the *bar* gene) were grown under long day condition (16/8 h light/dark) using cool-white fluorescence bulbs as the light resource at 23°C. Spraying treatments began upon the seed germination, and was repeated once every two days with approximately 0.4 mL **AA** solution per time per pot.

Structure determination of *holo*-pDHAD

The gene encoding pDHAD (residues 35–608) was cloned into pET21a derivative vector pSJ2 with an eight histidine (8×His) tag and a TEV protease cleavage site at the *N*-terminus. The following primers were used for cloning: the forward primer DHAD-F and the reverse primer DHAD-R. The double mutant K559A/K560A for efficient crystallization was designed using the surface entropy reduction prediction (SERp) server[34]. Mutations were generated by PCR using the forward primer K559AK560A-F and reverse primer K559AK560A-R. All constructed plasmids were verified by DNA sequencing.

pDHAD purified under aerobic conditions was found to contain no iron-sulfur cluster (*apo* form). Hence we performed [2Fe-2S] Cluster reconstitution under the atmosphere of nitrogen in an anaerobic box. The protein was incubated with $FeCl_3$ at the ratio of 1:10 for 1 h on ice and then 10 equivalents of Na_2S per protein was added drop-wise every 30 min for 3 h. The reaction mixture was then incubated overnight. Excess $FeCl_3$ and Na_2S were removed using a SephadexTM G-25 Fine column (GE Healthcare)[26].

The reconstituted *holo*-pDHAD was crystallized in an anaerobic box. The proteins (at 10 mg/mL) were mixed in a 1:1 ratio with the reservoir solution in a 50 μL volume of 2 μL and equilibrated against the reservoir solution, using the sitting-drop vapor diffusion method at 16°C. Crystals for diffraction were observed in 0.1 M sodium acetate pH 5.0, 1.5 M ammonium sulfate after 5 d.

All crystals were flash-cooled in liquid nitrogen after cryo-protected with solution containing 25% glycerol, 1.5 M ammonium sulfate, 0.1 M sodium acetate pH 5.0. The data were collected at 100K and at the Beam Line 19U1 in Shanghai Synchrotron Radiation Facility (SSRF). Diffraction data of *holo*-pDHAD was collected at the wavelength of 0.97774 Å. The best crystals diffracted to a resolution of 2.11 Å. The Ramachandran plot favored (%), allowed (%) and outlier (%) are 98.05, 1.60, and 0.36 respectively. All data sets were indexed, integrated, and scaled using the HKL3000 package[35]. The crystals belonged to space group $P4_22_12$. The statistics of the data collection are summarized in Extended Data Table 1.

The *holo*-pDHAD structure was solved by the molecular replacement method Phaser embedded in the CCP4i suite and the L-arabinonate dehydratase crystal structure (PDB_ID: 5J83) as the search model. All the side chains were removed during the molecular replacement process[36,37]. The resulting model were refined against the diffraction data using the REFMAC5 program of CCP4i[38]. Based on the improved electron density, the side chains of *holo*-pDHAD protein, iron sulfur cluster, water molecule, acetate ion, sulfate ions, and magnesium ion were manually built using the program WinCoot[39]. The R_{work} and R_{free} values of the structure are 17.67% and 22.15%, respectively. The detailed refinement statistics are summarized in Extended Data Table 1. The geometry of the model was validated by WinCoot. Structural factor and coordinate of *holo*-pDHAD have been deposited in the Protein Bank (PDB code: 5ZE4).

Homology modelling of AstD and docking of substrate or AA into active site of *holo*-pDHAD

The structure of *holo*-pDHAD was prepared in Schrodinger suite software under OPLS3 force field[40]. Hydrogen atoms were added to reconstituted crystal structures according to the physiological pH (7.0) with the PROPKA tool in Protein Preparation tool in Maestro to optimize the hydrogen bond network[26,41]. Constrained energy minimizations were conducted on the full-atomic models, with heavy atom coverage to 0.5 Å. The homology model was performed in Modeller 9.18[42], using the crystal structure of *holo*-pDHAD solved in this work as a template. Sequence alignment in Modeller indicated that AstD and pDHAD shared 56.8% sequence identity and 75.0% sequence similarity (Extended Data Fig. 6). All the highly conserved residues and motifs were properly aligned. A total of 2000 models were generated for each target in Modeller with the fully annealed protocol. The optimal models were chosen for docking studies according to DOPE (Discrete Optimized Protein Energy) score.

All ligand structures were built in Schrodinger Maestro software[26]. The LigPrep module in Schrodinger software was introduced for geometric optimization by using OPLS3 force field[40]. The ionization state of ligands were calculated with Epik tool employing Hammett and Taft methods in conjunction with ionization and tautomerization tools[43]. The docking of a ligand to the receptor was performed using Glide[44]. We included cofactors observed in crystal structure during the docking. Since both water and SO_4^{2-} occupied the catalytic site, they were excluded prior to docking. Cubic boxes centered on the ligand mass center with a radius 8 Å for all ligands defined the docking binding regions. Flexible ligand docking was

executed for all structures. Ten poses per ligand out of 20,000 were included in the post-docking energy minimization. The best scored pose for the ligand was chosen as the initial structure for further study. The MM/GBSA method was introduced to evaluate the ligand binding affinity based on the best scored docking pose in Schrodinger software. Figures are prepared in PyMOL and Inkscape[45,46]. Both of native substrate α,β-dihydroxyisovalerate and **AA** were docked into the catalytic site of pDHAD. The cross-section electrostatic surface map shows this unique catalytic pocket has a positively charged internal and a hydrophobic entrance, which binds to negatively charged "head" and hydrophobic "tail" of substrate or **AA** respectively. Thus the negatively charged "head" can lead both of the substrate and **AA** into the catalytic chamber. The bulky hydrophobic tricyclic moiety of **AA**, however, provides stronger hydrophobic interactions to the entrance and blocks the entrance of active site due to the hydrophobic residues at the entrance, including G68, A71, I72, I134, A133, M141, V212, F215, M498 and P501. In contrast, the smaller "tail" of native substrate provides less interactions to entrance because the smaller size limits efficient hydrophobic contact to nearby residues. This implies that once **AA** binds to pDHAD, it can prevent substrate approaching the active site. We also introduced molecular mechanics generalized Born and surface area (MM/GBSA) continuum solvation method, an widely used approach for relative binding energy calculation, to evaluate the relative binding affinity for both ligands[47]. The MM/GBSA calculations had been done in Prime[48] (Schrödinger 2015 suite). The MM/GBSA energy was calculated using following equation:

$$\Delta G_{bind} = E_{complex} - E_{protein} - E_{ligand}$$

E denotes energy and includes terms such as protein–ligand van der Waals contacts, electrostatic interactions, ligand desolvation, and internal strain (ligand and protein) energies, using VSGB2.0 implicit solvent model with the OPLS2005 force field. The solvent entropy is also included in the VSGB2.0 energy model, as it is for other Generalized Born (GB) and Poison–Boltzmann (PB) continuum solvent models.

MM/GBSA calculation shows that the relative binding energy for **AA** and α,β-dihydroxyisovalerate is −18.6 ± 0.3 kcal/mol and −13.3 ± 0.2 kcal/mol respectively, which shows the binding constant of **AA** to active site is about 6000 times greater than α,β-dihydroxyisovalerate. This further confirms that **AA** is a competitive inhibitor of pDHAD.

Cytotoxicity assay of AA

Cell proliferation experiments were performed in a 96-well format (five replicates per sample) using melanoma cell line A375 and SK-MEL-1. **AA** treatments were initiated 24 h postseeding for 72 h, and cell survival was quantified using CellTiter-GLO assay (Promega).

Cross experiment of *A. thaliana*

To make male sterile *A. thaliana*, **AA** was added to chemical hybridization agent (CHA) formulation (250 μM **AA**, 2% ethanol, 0.1% Tween-80, 1% corn oil in water), which has less inhibition effect on the growth of *A. thaliana*. Flowers of the **AA** treated col-0 were selected as the female parent. The non-treated *A. thaliana* containing a glufosinate resistant

gene were used as male parent to donate pollen. 2-week old F1 progeny resulting from the cross were treated by Finale (11.3% glufosinate-ammonium) at 1:2000 dilution. The results are summarized in Extended Data Fig. 9.

Construction of the transgenic plants

The coding sequence of AstD was codon optimized for *A. thaliana*. A chloroplast localization signal (CLS) of 35-amino acid residues derived from the *N*-terminal of *A. thaliana* DHAD (MQATIFSPRATLFPCKPLLPSHNVNSRRPSIISCS) was fused to N-terminus of the codon optimized AstD. A 3×FLAG-tag was inserted between the CLS and the codon optimized AstD (Supplementary Table 6). The gene block containing CLS, FLAG-tag and *astD* was synthesized and then cloned into pEG202 vector using Gateway LR Clonase II Enzyme Mix (ThermoFisher scientific). The original CaMV 35S promoter of pEG202 was substituted by Ubiquitin-10 promoter to drive the expression of AstD. The construct was electro-transformed into *Agrobacterium tumefaciens* strain Agl0 followed by *A. thaliana* transformation using the standard floral dip method[49]. The *A. thaliana* Col-0 ecotype was transformed. Positive transgenic plants were selected using the glufosinate resistance marker, and were tested for survival in presence of **AA**.

Protein expression verification with western blot

Approximately 0.5 gram of leaf tissue of transgenic *A. thaliana* was grounded in liquid nitrogen. Proteins were homogenized in 2× SDS buffer followed by 5-min centrifuge at 21,000 g to remove undissolved debris. The supernatant containing resolved proteins were loaded onto a 4–12% Bis-Tris gel, and separated using MOPS running buffer. Transfer was conducted using iBlot2 dry transfer device and PVDF membrane. The total proteins were stained with Ponceau to demonstrate equal loading. Western blotting was performed using Sigma monoclonal anti-FLAG M2-Peroxidase antibody, followed by detection using Amersham ECL Prime detection reagent.

Data availability

The data that support the findings of this study are available within the paper and its Supplementary Information, or are available from the corresponding authors upon reasonable request.

Extended Data

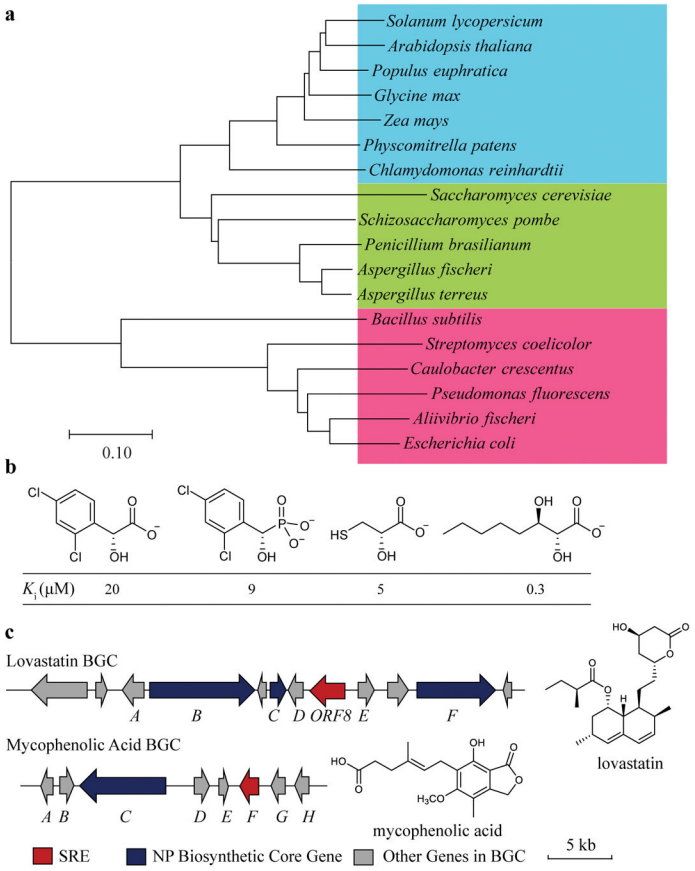

Extended Data Figure 1. The rationale of resistance-gene directed discovery of a natural herbicide with new mode of action

a, Phylogenetic tree of DHAD among bacteria, fungi and plants. The evolutionary history was inferred by using the Neighbor-Joining method (MEGA7). Units represent the number of amino acid substitutions per site. **b,** Representatives of small molecules that inhibit DHAD *in vitro*, but fail to inhibit plant growth. **c,** Examples of co-localization of biosynthetic gene clusters (BGCs) and targets. The biosynthetic core genes are shown in blue and the self-resistance enzymes (SREs) are shown in red. The blockbuster cholesterol-lowering lovastatin drug targets HMG-CoA reductase (HMGR) in eukaryotes. In the fungus *Aspergillus terreus* that produces lovastatin, a second copy of HMGR encoded by ORF8 is present in the gene cluster (top). BGC of the immunosuppressant mycophenolic acid from *Penicillium sp.* contains a second copy of inosine monophosphate dehydrogenase (IMPDH), which represents the SRE to this cluster (bottom).

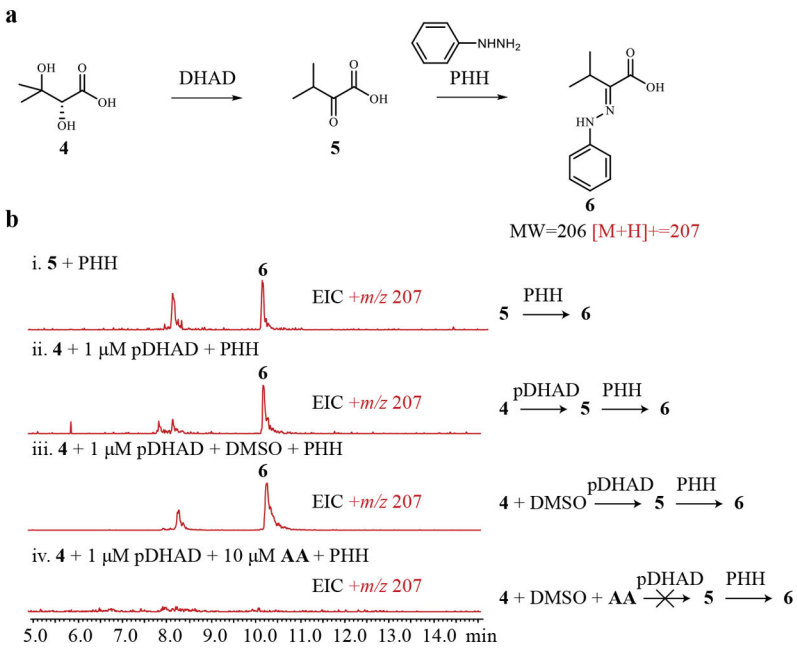

Extended Data Figure 2. Biochemical assays of DHAD functions

a, Assaying DHAD activities in converting the dihydroxyacid **4** into the α-ketoacid **5.** Formation of **5** can be detected on HPLC by chemical derivatization using phenylhydrazine (PHH) to yield **6. b,** LC-MS traces of the biochemical assays of *A. thaliana* DHAD (pDHAD). Extracted ion chromatogram (EIC) of positive ion mass of $[M+H]^+$=207 is shown in red. i. The derivatization reaction was validated by using the authentic **5**. ii. The bioactivity of pDHAD in converting **4** into **5** was validated. iii. Addition of DMSO to pDHAD enzymatic reaction mixture has no effect. iv. Addition of 10 μM **AA** to the reaction mixture abolished pDHAD activity. The experiments were repeated independently for 3 times with similar results.

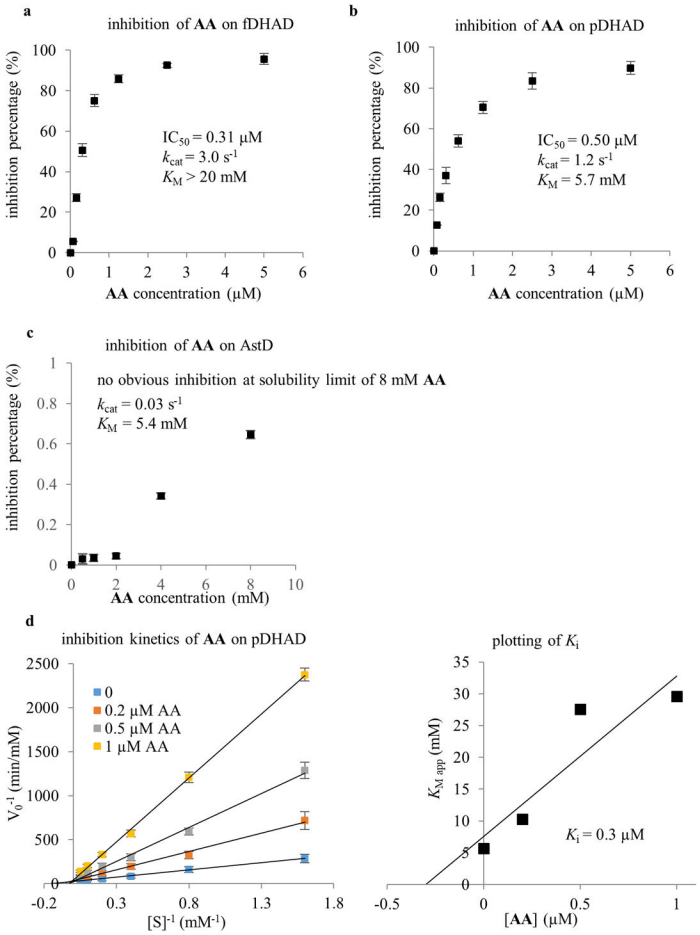

Extended Data Figure 3. Inhibition assay of different DHADs using AA

Three DHAD enzymes were assayed, including pDHAD (**p**lant DHAD from *A. thaliana*), fDHAD (**f**ungal housekeeping DHAD from *A. terreus*) and AstD (DHAD homolog within *ast* cluster). IC_{50} and K_i values of **AA** were measured based on inhibition percentage at different **AA** concentrations. Center values are averages, errors bars are s.d.; n = 3 biologically independent experiments. **a,** Plot of the inhibition percentage of 0.5 μM fDHAD as a function of **AA** concentration**. b,** Plot of the inhibition percentage of 0.5 μM pDHAD as a function of **AA** concentration**. c,** Plot of the inhibition percentage of 0.5 μM AstD as a function of **AA** concentration**. d,** Analysis of inhibitory kinetics of **AA** on pDHAD using the Lineweaver-Burk method at different concentrations of **AA** (left). Linear fitting of apparent Michaelis constant ($K_{M,app}$) as a function of **AA** concentration yields the inhibition constant (K_i) of **AA** on pDHAD (right).

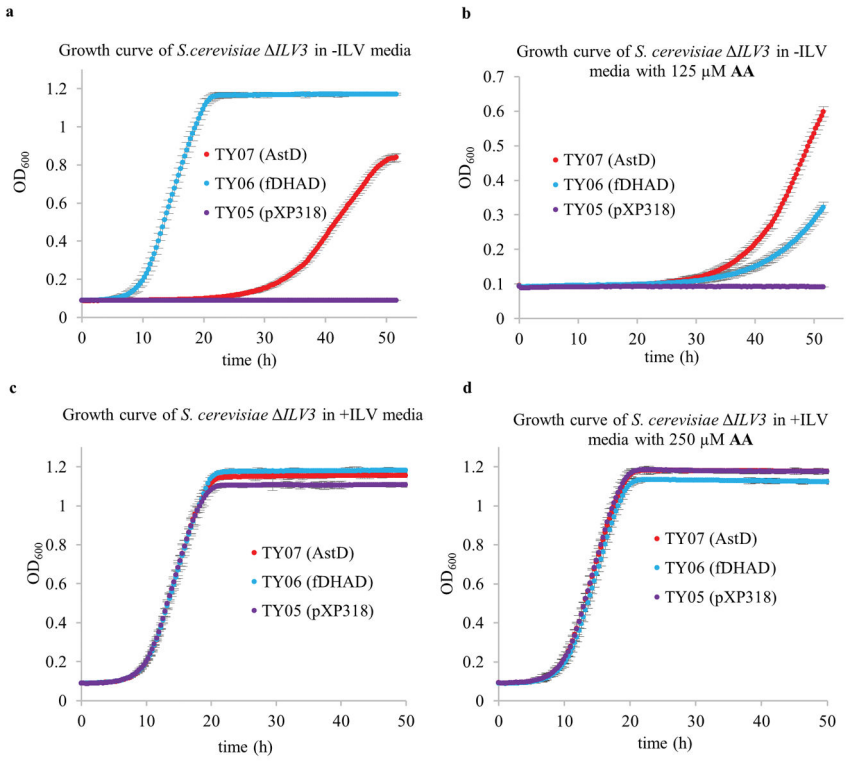

Extended Data Figure 4. Growth curve of *S. cerevisiae* Δ*ILV3* expressing AstD and fDHAD

The genome copy of DHAD encoded by *ILV3* was first deleted from *Saccharomyces cerevisiae* strain DHY Δ*URA3* to give UB02. UB02 was then either chemically complemented by growth on ILV (leucine, isoleucine and valine)-containing media or genetically by expressing of fDHAD or AstD episomally (TY06 or TY07, respectively). The empty vector pXP318 was also transformed into UB02 to generate a control strain TY05. The optical density of cell growth under different conditions were plotted as a function of time. Center values are averages, errors bars are s.d.; n = 3 biologically independent experiments. **a,** Growth curve in ILV dropout media with no **AA. b,** Growth curve in ILV dropout media with 125 μM **AA. c,** Growth curve in ILV supplemented media; **d,** Growth curve in ILV supplemented media with 250 μM **AA**.

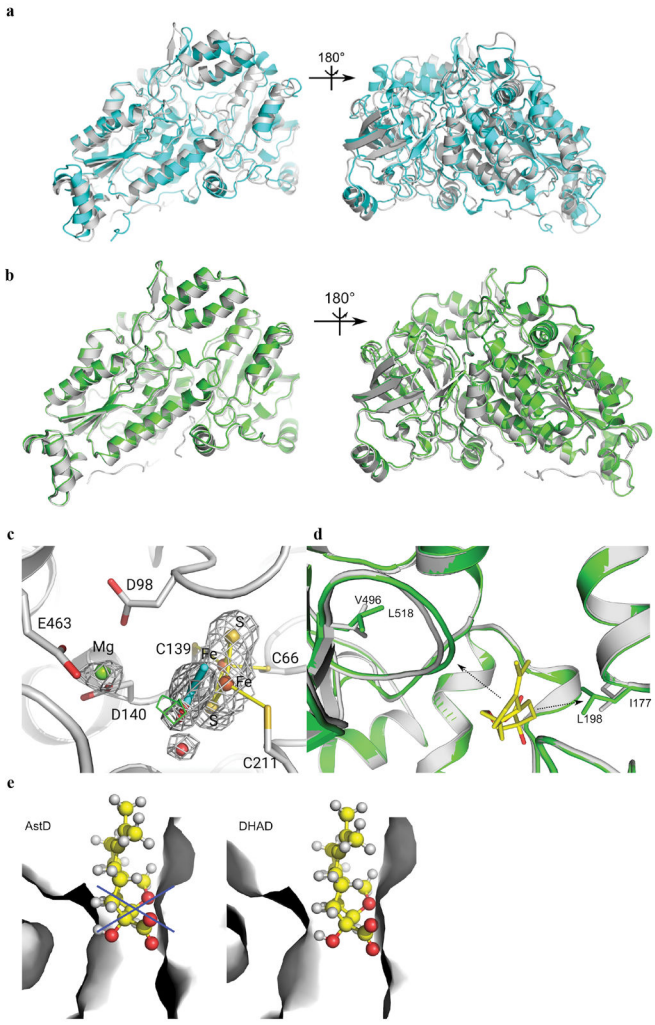

Extended Data Figure 5. X-ray Structure of *holo*-pDHAD and homology model of AstD

a, Superimpositions monomer of *holo*-pDHAD (PDB: 5ZE4, 2.11 Å) and RlArDHT (PDB: 5J84). The *holo* structure containing the 2Fe-2S cofactor and Mg^{2+} ion in the active site. The structure of *holo*-pDHAD is in white; the crystal structure of RlArDHT is in cyan. **b,** Superimpositions of *holo*-pDHAD and homology modeled AstD. The structure of AstD was constructed by homology modeling based on the structure of *holo*-pDHAD. The structure of *holo*-pDHAD is in white; the crystal structure of AstD is in green. **c,** The electron density map of cofactors in the *holo* structure of pDHAD. White grid: 2Fo-Fc map at 1.2 σ level. Green grid: Fo-Fc positive map at 3.2σ level. Cyan sticks: acetic acid molecule. **d,** Comparison of the active sites in the crystal structure of pDHAD and the modeled structure of AstD. The cartoon represents superimposed binding sites of pDHAD (white) and AstD (green). The shift of a loop in AstD, where L518 (correspond to V496 in pDHAD) is located, coupled with a larger L198 residue (correspond to I177 in pDHAD) lead to a smaller hydrophobic pocket of AstD than that in pDHAD. **e,** The surface of binding sites of AstD (left) and pDHAD (right). The smaller hydrophobic channel in modeled AstD cannot accommodate the **AA** molecule (yellow balls-and-sticks).

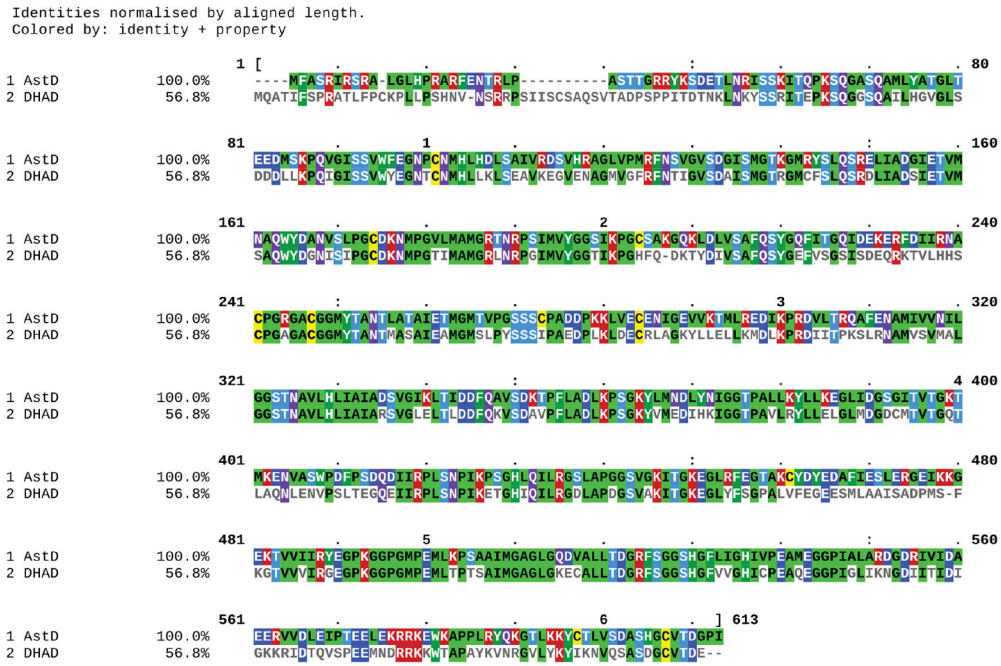

Extended Data Figure 6. Sequence alignment between pDHAD and AstD

The sequence identity between pDHAD and AstD is 56.8%, whereas the similarity between them is 75.0%. Residues were colored according to their property and similarity.

Extended Data Figure 7. Spray assay of AA on *A. thaliana*

Glufosinate resistant *A. thaliana* was treated with (right) or without (left) **AA** in the solvent, which is a commercial glufosinate based herbicide marketed as Finale®. To improve the wetting and penetration, **AA** was firstly dissolved in ethanol and then added to solvent (0.06 g/L Finale® Bayer Inc. + 20 g/L ethanol) to make 250 μM **AA** spraying solution. The

control plants were treated with solvent containing ethanol only. Spraying treatments began upon the seeds germination, and were repeated once every two days with approximately 0.4 mL **AA** solution per time per pot for 4 weeks. The picture shown below is taken after one month of treatment. The application rate of **AA** is approximately 1.6 lb/acre, which is comparable to the commonly used herbicide glyphosate (0.75~1.5 lb/acre). The experiments were repeated independently for 3 times with similar results.

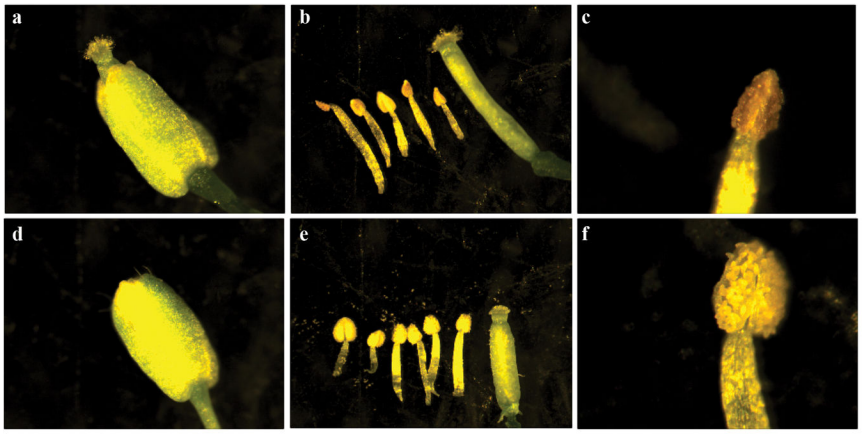

Extended Data Figure 8. Specific inhibition of anther development in *A. thaliana*

Comparison of flower organs between the **AA** treated (**a–c**) and non-treated (**d–f**) *Arabidopsis*. **a** compare to **d**, the **AA** treated flower shows abnormal pistil elongation due to the lack of pollination. **b** compare to **e**, the **AA** treated flower is missing one stamen. **c** compare to **f**, the **AA** treated anther is depleted of healthy and mature pollen. The experiments were performed twice with similar results.

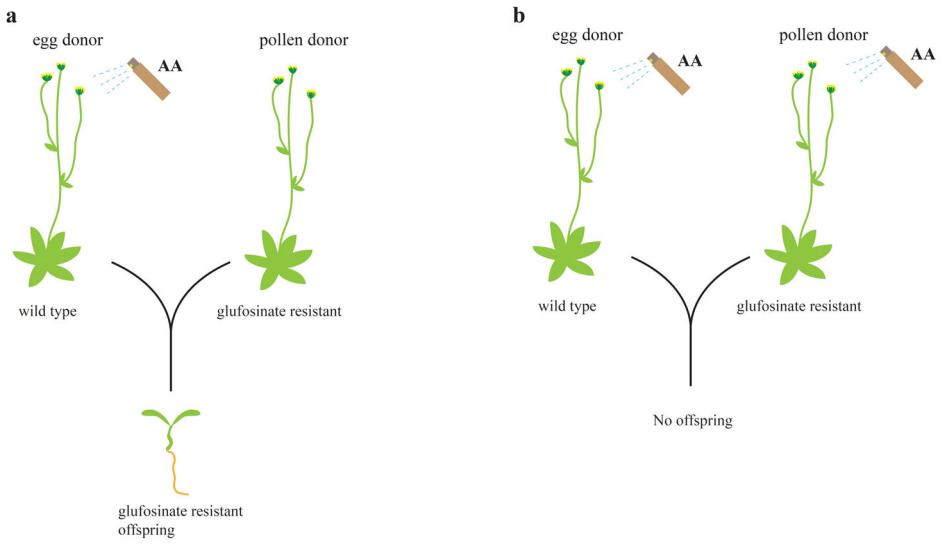

female parent	male parent	offspring obtained	inherit resistance
AA treated wild type	un-treated Glufosinate resistant plant	Yes	Yes
AA treated wild type	**AA** treated glufosinate resistant plant	No	N/A

Extended Data Figure 9. Schematic illustration of results from the cross experiment

a, Wild type *A. thaliana* treated with 250 μM **AA** was pollinated with pollen from the un-treated plant that carries the glufosinate resistant gene. Offspring was obtained, and inherited the glufosinate resistance from the pollen donor. **b,** similar as in **a**, except that the pollen donor was also treated with 250 μM **AA**. No offspring was obtained from this cross. Similar results were obtained with the treatment of **AA** at 100 μM.

Extended Data Table 1

Data collection and refinement statistics (molecular replacement).

	***holo*-pDHAD**
Data collection	
Space group	$P4_22_12$
Cell dimensions	
a, b, c (Å)	135.5, 135.5, 66.0
α, β, γ (°)	90, 90, 90
Resolution (Å)	47.89-2.11 (2.15-2.11) *
R_{sym} or R_{merge}	0.189 (1.240)
$I/\sigma I$	17.86 (2.33)
Completeness (%)	100 (100)
Redundancy	25.1 (23.1)
Refinement	

	***holo*-pDHAD**
Resolution (Å)	95.79-2.11
No. reflections	33235 (1714)
R_{work}/R_{free}	0.1767/0.2216
No. atoms	
Protein	4208
Ligand/ion	24
Water	118
B-factors	
Protein	26.60
Ligand/ion	46.53
Water	26.22
R.m.s. deviations	
Bond lengths (Å)	0.007
Bond angles (°)	1.195

*Values in parentheses are for highest-resolution shell.

Supplementary Material

Refer to Web version on PubMed Central for supplementary material.

Acknowledgments

This work was supported by the NIH (1DP1GM106413 and 1R35GM118056) to Y.T. and CAS (XDB20000000) to J.Z.. S.E.J is an Investigator of the Howard Hughes Medical Institute. Q.L. is supported by the NIH (F32) Postdoctoral Fellowship. We thank Stanford Genome Technology Center for the *Saccharomyces cerevisiae* DHY *ΔURA3* strain. The diffraction data of *holo*-pDHAD was collected at beamline BL19U1 in Shanghai Synchrotron Radiation Facility (SSRF). The molecular modeling was performed at the Interdisciplinary Centre for Mathematical and Computational Modeling in Warsaw (GB70-3 & GB71-3). We thank assistance from Dr. Weixue Huang, Ms. Lian Wu, and Ms. Rong Cheng for technical help in protein purification and crystallization.

References

1. Dayan FE, Duke SO. Natural compounds as next generation herbicides. Plant Physiol. 2014; 166:1090–1105. [PubMed: 24784133]
2. Newman DJ, Cragg GM. Natural products as sources of new drugs from 1981 to 2014. J Nat Prod. 2016; 79:629–661. [PubMed: 26852623]
3. Jon C, Christopher W. Lessons from natural molecules. Nature. 2004; 432:829–837. [PubMed: 15602548]
4. Ziemert N, Alanjary M, Weber T. The evolution of genome mining in microbes - a review. Nat Prod Rep. 2016; 33:988–1005. [PubMed: 27272205]
5. Clevenger KD, et al. A scalable platform to identify fungal secondary metabolites and their gene clusters. Nat Chem Biol. 2017; 13:895. [PubMed: 28604695]
6. Rutledge PJ, Challis GL. Discovery of microbial natural products by activation of silent biosynthetic gene clusters. Nat Rev Microbiol. 2015; 13:509. [PubMed: 26119570]
7. Tang X, et al. Identification of thiotetronic acid antibiotic biosynthetic pathways by target-directed genome mining. ACS Chem Biol. 2015; 10:2841–2849. [PubMed: 26458099]
8. Alanjary M, et al. The antibiotic resistant target seeker (ARTS), an exploration engine for antibiotic cluster prioritization and novel drug target discovery. Nucleic Acids Res. 2017; 45:W42–W48. [PubMed: 28472505]

9. Yeh HH, et al. Resistance gene-guided genome mining: serial promoter exchanges in *Aspergillus nidulans* reveal the biosynthetic pathway for fellutamide B, a proteasome inhibitor. ACS Chem Biol. 2016; 11:2275–2284. [PubMed: 27294372]
10. Amorim Franco TM, Blanchard JS. Bacterial branched-chain amino acid biosynthesis: structures, mechanisms, and drugability. Biochemistry. 2017; 56:5849–5865. [PubMed: 28977745]
11. Heap I. Global perspective of herbicide-resistant weeds. Pest Manag Sci. 2014; 70:1306–1315. [PubMed: 24302673]
12. Soltani N, et al. Potential corn yield losses from weeds in north america. Weed Technol. 2016; 30:979–984.
13. Swanton CJ, Harker KN, Anderson RL. Crop losses due to weeds in Canada. Weed Technol. 1993; 7:537–542.
14. Gianessi LP. The increasing importance of herbicides in worldwide crop production. Pest Manag Sci. 2013; 69:1099–1105. [PubMed: 23794176]
15. Flint DH, Emptage MH. Dihydroxy acid dehydratase from spinach contains a [2Fe-2S] cluster. J Biol Chem. 1988; 263:3558–3564. [PubMed: 2831190]
16. Flint DH, Emptage MH, Finnegan MG, Fu W, Johnson MK. The role and properties of the iron-sulfur cluster in *Escherichia coli* dihydroxy-acid dehydratase. J Biol Chem. 1993; 268:14732–14742. [PubMed: 8325851]
17. Flint DH, Nudelman A. Studies on the active site of dihydroxy-acid dehydratase. Bioorg Chem. 1993; 21:367–385.
18. Pusztahelyi T, Holb I, Pócsi I. Secondary metabolites in fungus-plant interactions. Front Plant Sci. 2015; 6:573. [PubMed: 26300892]
19. Kennedy Jonathan, et al. Modulation of polyketide synthase activity by accessory proteins during lovastatin biosynthesis. Science. 1999; 284:1368–1372. [PubMed: 10334994]
20. Regueira TB, et al. Molecular basis for mycophenolic acid biosynthesis in *Penicillium brevicompactum*. Appl Environ Microbiol. 2011; 77:3035–3043. [PubMed: 21398490]
21. Fischbach MA, Walsh CT. Assembly-line enzymology for polyketide and nonribosomal peptide antibiotics: logic, machinery, and mechanisms. Chem Rev. 2006; 106:3468–3496. [PubMed: 16895337]
22. Christianson DW. Structural biology and chemistry of the terpenoid cyclases. Chem Rev. 2006; 106:3412–3442. [PubMed: 16895335]
23. Tang MC, et al. Discovery of unclustered fungal indole diterpene biosynthetic pathways through combinatorial pathway reassembly in engineered yeast. J Am Chem Soc. 2015; 137:13724–13727. [PubMed: 26469304]
24. Tsuda Yoshisuke. Aspterric acid, a new sesquiterpenoid of the carotane group, a metabolite from Aspergillus terreus IFO-6123. X-Ray crystal and molecular structure of its p-bromobenzoate. J Chem Soc, Chem Commun. 1978:160–161.
25. Shimada A, et al. Aspterric acid and 6-hydroxymellein, inhibitors of pollen development in *Arabidopsis thaliana*, produced by *Aspergillus terreus*. Z Naturforsch C. 2002; 57:459–464. [PubMed: 12132685]
26. Rahman MM, et al. The crystal structure of a bacterial L-arabinonate dehydratase contains a [2Fe-2S] cluster. ACS Chem Biol. 2017; 12:1919–1927. [PubMed: 28574691]
27. Kirkwood RC. Use and mode of action of adjuvants for herbicides: a review of some current work. Pestic Sci. 1993; 38:93–102.
28. Hoerlein G. Glufosinate (phosphinothricin), a natural amino acid with unexpected herbicidal properties. Rev Environ Contam Toxicol. 1994; 138:73–145. [PubMed: 7938785]
29. McRae DH. Plant Breeding Reviews. John Wiley & Sons, Inc; 1985. 169–191.
30. Benbrook CM. Trends in glyphosate herbicide use in the United States and globally. Environ Sci Eur. 2016; 28:3–19. [PubMed: 27752438]
31. Liu N, et al. Identification and heterologous production of a benzoyl-primed tricarboxylic acid polyketide intermediate from the zaragozic acid A biosynthetic pathway. Org Lett. 2017; 19:3560–3563. [PubMed: 28605916]

32. Fang F, et al. A vector set for systematic metabolic engineering in *Saccharomyces cerevisiae*. Yeast. 2011; 28:123–136. [PubMed: 20936606]
33. Cool LG. ent-Daucane and acorane sesquiterpenes from *Cupressocyparis leylandii* foliage. Phytochemistry. 2001; 58:969–972. [PubMed: 11684197]
34. Goldschmidt L, Cooper DR, Derewenda ZS, Eisenberg D. Toward rational protein crystallization: a web server for the design of crystallizable protein variants. Protein Sci. 2007; 16:1569–1576. [PubMed: 17656576]
35. Otwinowski Z, Minor W, WCC. Processing of X-ray diffraction data collected in oscillation mode. Methods Enzymol. 1997; 276:307–326.
36. McCoy AJ, et al. Phaser crystallographic software. Journal of applied crystallography. 2007; 40:658–674. [PubMed: 19461840]
37. Winn MD, et al. Overview of the CCP4 suite and current developments. Acta crystallographica Section D, Biological crystallography. 2011; 67:235–242. [PubMed: 21460441]
38. Murshudov GN, et al. REFMAC5 for the refinement of macromolecular crystal structures. Acta crystallographica Section D, Biological crystallography. 2011; 67:355–367. [PubMed: 21460454]
39. Emsley P, Lohkamp B, Scott WG, Cowtan K. Features and development of Coot. Acta crystallographica Section D, Biological crystallography. 2010; 66:486–501. [PubMed: 20383002]
40. Harder E, et al. OPLS3: a force field providing broad coverage of drug-like small molecules and proteins. J Chem Theory Comput. 2016; 12:281–296. [PubMed: 26584231]
41. Søndergaard CR, Olsson MHM, Rostkowski M, Jensen JH. Improved treatment of ligands and coupling effects in empirical calculation and rationalization of pKa values. J Chem Theory Comput. 2011; 7:2284–2295. [PubMed: 26606496]
42. Eswar N, et al. Comparative protein structure modeling using Modeller. Current protocols in bioinformatics/editoral board, Andreas D. Baxevanis … [et al.]. 2006; Chapter 5(Unit 5):6.
43. Greenwood JR, Calkins D, Sullivan AP, Shelley JC. Towards the comprehensive, rapid, and accurate prediction of the favorable tautomeric states of drug-like molecules in aqueous solution. J Comput Aided Mol Des. 2010; 24:591–604. [PubMed: 20354892]
44. Friesner RA, et al. Glide: a new approach for rapid, accurate docking and scoring. 1 method and assessment of docking Accuracy. J Med Chem. 2004; 47:1739–1749. [PubMed: 15027865]
45. Yuan S, Chan HCS, Filipek S, Vogel H. PyMOL and Inkscape bridge the data and the data visualization. Structure. 2016; 24:2041–2042. [PubMed: 27926832]
46. Yuan S, Chan HCS, Hu Z. Using PyMOL as a platform for computational drug design. Wiley Interdiscip Rev Comput Mol Sci. 2017; 7:e1298. n/a.
47. Genheden S, Ryde U. The MM/PBSA and MM/GBSA methods to estimate ligand-binding affinities. Expert Opin Drug Discov. 2015; 10:449–461. [PubMed: 25835573]
48. Sirin S, et al. A computational approach to enzyme design: predicting ω-aminotransferase catalytic activity using docking and MM-GBSA scoring. J Chem Inf Model. 2014; 54:2334–2346. [PubMed: 25005922]
49. Clough SJ, Bent AF. Floral dip: a simplified method for *Agrobacterium*-mediated transformation of *Arabidopsis thaliana*. Plant J. 1998; 16:735–743. [PubMed: 10069079]

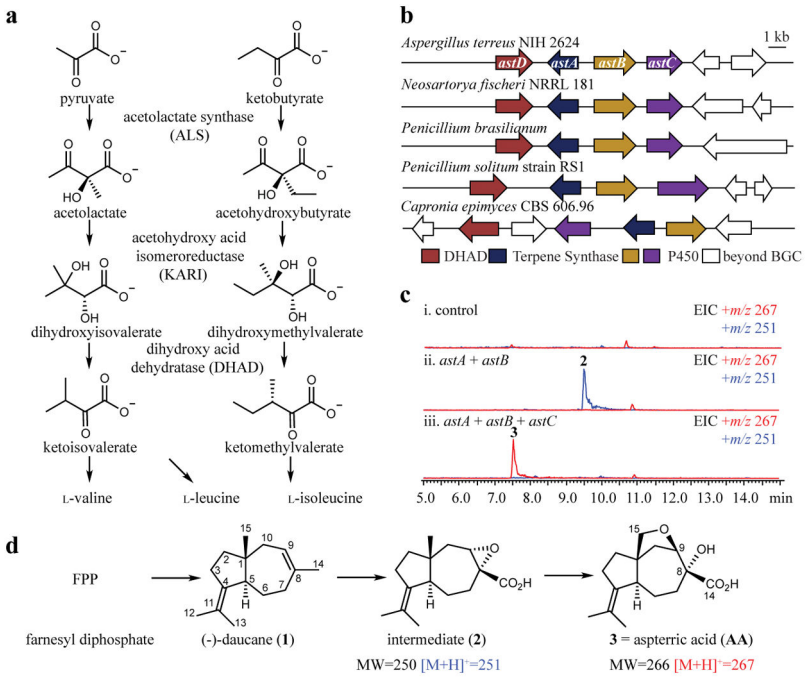

Fig. 1.

Genome mining of a DHAD inhibitor and biosynthesis of aspterric acid (**AA**). **a,** Valine, leucine and isoleucine are produced by two parallel pathways using three enzymatic steps: ALS, KARI, and DHAD. **b,** A 17 kb gene cluster from *A. terreus* containing four ORFs, which are also conserved among several fungal species. AstA has sequence homology to sesquiterpene cyclase; AstB and AstC are predicted to be P450 monooxygenases; *astD* is predicted to encode a DHAD, and is proposed to confer self-resistance in the presence of the NP produced in the cluster. **c,** HPLC-MS traces of metabolites produced from *S. cerevisiae* RC01 expressing different *ast* genes under P_{ADH2} promoter control. i: *S. cerevisiae* without expression plasmids. ii: *S. cerevisiae* transformed with plasmids expressing *astA* and *astB* produces **2**. iii: *S. cerevisiae* transformed with plasmids expressing *astA-C* produces **AA** at a titer of 20 mg/L. The experiments were repeated independently with similar results for 3 times. **d,** Proposed biosynthetic pathway of **AA**. AstA cyclizes farnesyl diphosphate (FPP) into (−)-daucane **1**, while the P450 enzymes AstB and AstC sequentially transform **1** into **2** and **3 (AA)**, respectively.

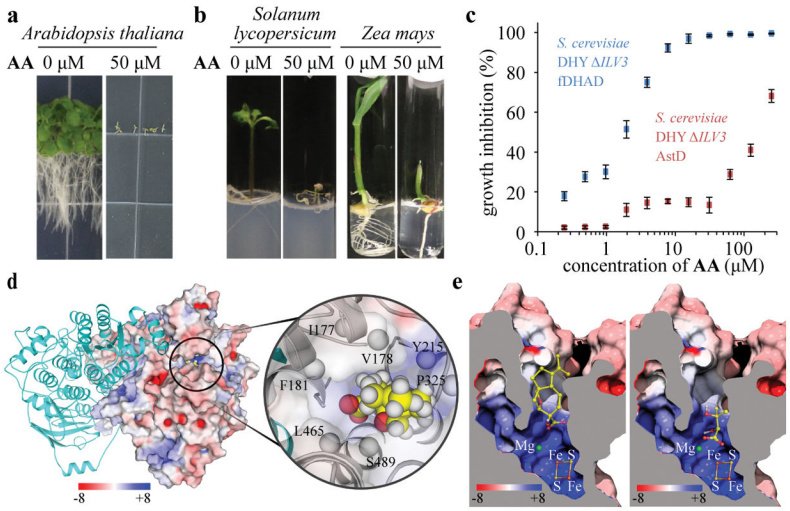

Fig. 2. Aspterric acid (AA) is a plant growth inhibitor

a, 2-week old *Arabidopsis thaliana* growing on MS media containing no **AA** (left) or 50 μM **AA** (right). The picture shown is representative of 3 replicates. **b,** Same as in **a**, except for 2-week old dicot *Solanum lycopersicum* and monocot *Zea mays*. The picture shown is representative of 2 replicates. **c,** Verification of the self-resistance function of AstD. Growth inhibition curve of **AA** on *S. cerevisiae* Δ*ILV3* strains expressing fungal housekeeping fDHAD (blue) or AstD (red) in isoleucine, leucine and valine (ILV) dropout media. The plot shows mean values ± s.d. (error bars); n = 3 biologically independent experiments. **d,** Crystal structure of the dimeric *holo A. thaliana* DHAD (pDHAD) containing the cofactor 2Fe-2S cluster and a Mg^{2+} ion with the docked **AA** in the active site. One of the pDHAD monomers is show in cyan, whereas the other one is shown in electrostatic surface representation. The docked **AA** is shown in the inset in spaced-filled model. The hydrophobic portions of **AA** are surrounded by several hydrophobic residues (white spheres) from both monomers. **e,** Cross-section electrostatic map of modeled *holo*-pDHAD in the binding site. Red map: the normalized negatively charged regions; blue map: the normalized positively charged regions; white map: the hydrophobic regions. The docked **AA** in the active site of pDHAD is shown on the left, while the docked native substrate dihydroxyisovalerate is shown on the right. The docking studies suggest the hydrophobic entrance to the reaction chamber preferentially binds the bulkier, tricyclic **AA.**

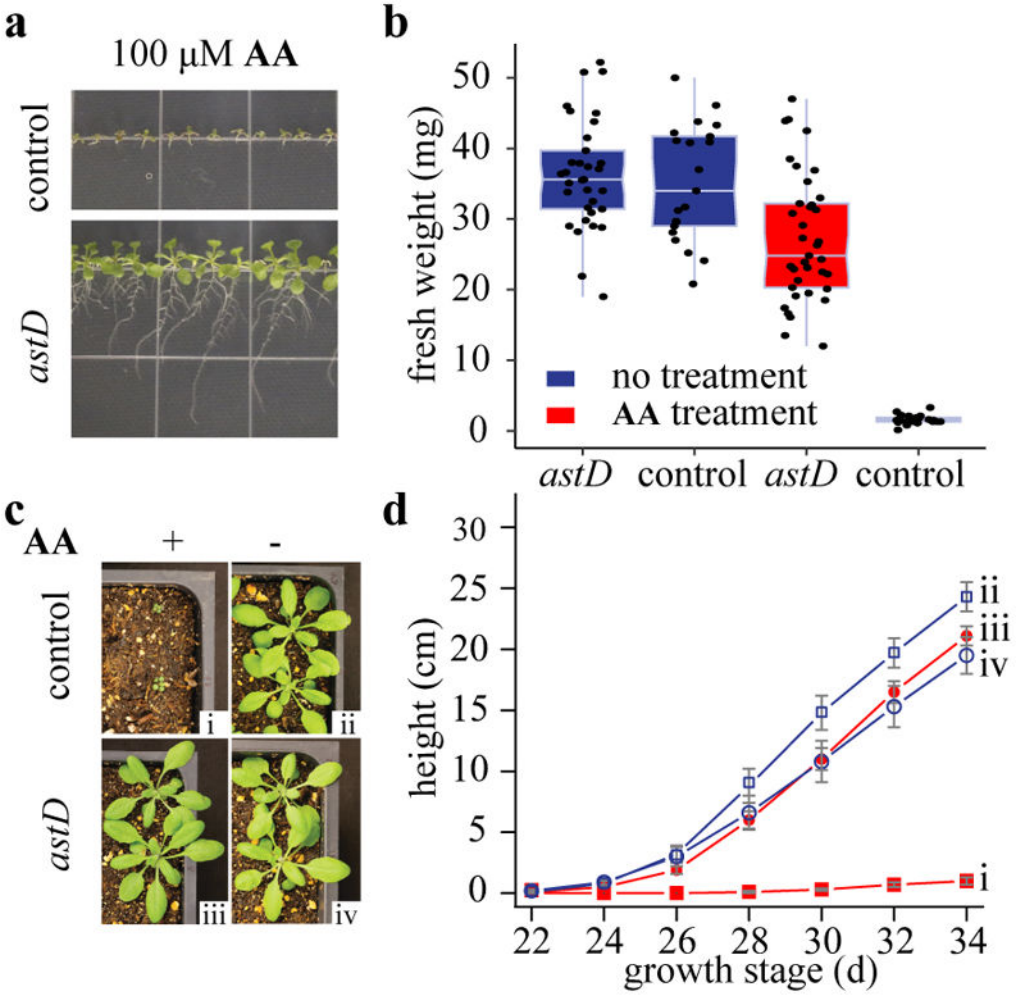

Fig. 3.

AA-resistance of *Arabidopsis* plants expressing *astD* transgenes. **a,** Phenotype of 10-day old *A. thaliana* with (lower) and without (upper) *astD* transgene growing on media containing 100 µM **AA**. Control plants were transformed with a vector that carries the glufosinate ammonium selection marker but no *astD* transgene. The picture shown is representative of 3 replicates. **b,** Fresh weight of 3-week old *Arabidopsis* seedlings growing on media with (red box) and without (blue box) 100 µM **AA**; Box plots show the median and extend of the 1st to 3rd quartile range, with individual data points overlaid; n = 21 biologically independent experiments. **c,** glufosinate-resistant *Arabidopsis* with (lower) and without (upper) *astD* transgene growing in soil were sprayed with glufosinate ammonium with (left) and without (right) 250 µM **AA.** i. control sprayed with 250 µM **AA** + glufosinate ammonium. ii. control sprayed with glufosinate ammonium only. iii. *astD* transgenic *Arabidopsis* sprayed with 250 µM **AA** + glufosinate ammonium. iv. *astD* transgenic *Arabidopsis* sprayed with glufosinate ammonium only. The picture shown is representative of 3 replicates. **d,** Quantification of the height of *Arabidopsis* treated the same as in **c**; The plot shows mean values ± s.d. (error bars); n = 12 biologically independent experiments.